catalysts

MDPI

Review

Development of Adsorptive Materials for Selective Removal of Toxic Metals in Wastewater: A Review

Moeng Geluk Motitswe [1], Kassim Olasunkanmi Badmus [2,*] and Lindiwe Khotseng [1]

[1] Chemistry Department, University of the Western Cape, Cape Town 7535, South Africa
[2] Industrial Chemistry Department, First Technical University, Ibadan 200255, Nigeria
* Correspondence: kassim.badmus@tech-u.edu.ng; Tel.: +23-490-60397156

Abstract: Removal of toxic metals is essential to achieving sustainability in wastewater purification. The achievement of efficient treatment at a low cost can be seriously challenging. Adsorption methods have been successfully demonstrated for possession of capability in the achievement of the desirable sustainable wastewater treatment. This review provides insights into important conventional and unconventional materials for toxic metal removal from wastewater through the adsorption process. The importance of the role due to the application of nanomaterials such as metal oxides nanoparticle, carbon nanomaterials, and associated nanocomposite were presented. Besides, the principles of adsorption, classes of the adsorbent materials, as well as the mechanisms involved in the adsorption phenomena were discussed.

Keywords: adsorption; wastewater; nanocomposite; nanoparticle; metal-oxide

Citation: Motitswe, M.G.; Badmus, K.O.; Khotseng, L. Development of Adsorptive Materials for Selective Removal of Toxic Metals in Wastewater: A Review. *Catalysts* **2022**, *12*, 1057. https://doi.org/10.3390/catal12091057

Academic Editors: Fengxia Deng and Xiaoxiao Zhang

Received: 12 July 2022
Accepted: 26 August 2022
Published: 16 September 2022

1. Introduction

Water covers 71% of the Earth's surface and is essential for the well-being of biotic and abiotic species (plants, soils, humans, and animals). Rapid global urbanization has led to increased pressure on water demands. The small amount of freshwater (3%) on Earth's crust is available for human use, whereas most of the freshwater is trapped in the ice caps and glaciers (makes 68.7% of 3% of available freshwater on Earth) [1]. However, water contamination and management (use and treatment) are significant challenges worldwide.

Amongst the pollutants, toxic metals are reported to possess a non-biodegradable, persistent, highly stable, water-soluble, and recalcitrant nature in water media, making the efficiency of remediation methods complex [2–4]. The toxic metals contaminations can be caused by human anthropogenic activities (battery, tannery, textile, domestic sewages, mine and smelting industries, etc.) and natural occurrences (stormwater runoff/s, volcanic eruptions, mineral weathering, forest fires, soil erosion, etc.) [5–7]. They are described as metals with a density equal to or greater than 5 g/cm^3, an atomic number greater than 11, and the tendency for metals to bio-accumulate in both living and non-living matters, posing chronic and acute health risks. The immediate effect of the toxic metals in the environment is marine ecosystem disintegration and soil degradation [8].

The remediation of toxic metal-contaminated wastewater needs good quality, selective, stable (catalytic, thermal, mechanical), reproducible and reusable materials to be employed in treatment systems [9,10]. Several treatment methods, namely, membrane technology, flocculation, coagulation/flocculation, chemical precipitation, ion exchange, electrochemical methods, phytoremediation, and biological methods, have been used for water and wastewater remediation [11,12].

Most current conventional methods are ineffective for toxic metal removal in the range of 1–100 mg/L. Besides, they are associated with demerits such as expensive disposal procedures, elevated chemical use, high energy consumption, a large formation of sludge/secondary pollutants, and sensitive operating conditions [13]. In overcoming these drawbacks, adsorption methods have proven more suitable, practical, and proficient for

toxic metal removal in wastewater due to fast kinetics, high uptake capacities, efficiencies, selectivity, and simplicity [14]. The process is based on the net metal accumulation at the surface of the solid phase (adsorbent), and the efficiency is more attributed to the adsorbent's nature. The adsorption consists of three phases: transport of the adsorbate from the liquid phase to the solid adsorbent surface, adsorption of the analytes onto the solid adsorbent surface, and transportation of adsorbate within the adsorbent particle [13]. Consequently, the current paper presents adsorption processes as an efficient method for removing toxic metal contaminants from wastewater. The different classes of materials, as well as the principle of adsorption, were also discussed.

2. Types of Adsorption

The adsorption types are chemisorption and physisorption (Table 1). The chemisorption is the binding of the adsorbate onto the adsorbent surface through strong ionic or covalent bonds. The factors such as pH, contact time, ionic strength, temperature, and adsorbent dosage can affect its efficiency [15,16]. Meanwhile, the physisorption occurs due to weak electrostatic interactions involving dipole-dipole, van der Waals, and London force [17,18]. The Dubinin–Radushkevish, Freundlich, Brunauer–Emmet–Teller, Jovanovich, Linear, Redlich–Peterson, and Temkin adsorption isotherms are essential models employed to differentiate physisorption from chemisorption isotherms (Langmuir, Sips, Volmer, Redlich–Peterson) [19,20].

Table 1. Merits and demerits of the chemisorption and physisorption.

Chemisorption	Physisorption
Ideal for single-layer adsorption	Suitable for multilayer adsorption
Irreversible sorption	Reversible sorption
Best fit for monolayer (homogeneous system)	Suitable for non-ideal (heterogeneous system)
Highly specific bonding	Non-specific bonding
Strong process	Weak process
Effective for chemical bonding	Effective for physical bonding
Slow adsorption at low temperature	Fast adsorption at low temperature
Not suitable for multilayer adsorption Costly due to the irreversibility Large adsorption enthalpy Not reusable	Suitable for multilayer adsorption Inexpensive due to desorption Low activation energy Reusable

3. Adsorption Isotherm and Kinetic

The adsorption kinetics and isotherm models are described in this review to better understand the adsorptive materials' performance toward the adsorbates. These models are ranked from weak to suitable components for a thorough understanding of chemisorption and physisorption [21].

3.1. Adsorption Isotherm Model

The isotherm models describe the relationship between the liquid state equilibrium adsorbate and the amount of equilibrium adsorption on the solid state at a specific temperature (Table 2). These isotherms are readily helpful for analyzing the adsorbent's adsorption capacities and efficiencies. The adsorption isotherms have been determined through numerous models: Langmuir, Freundlich, Sips, Dubinin–Radushkevish, Linear (Henry's Law), Redlich–Peterson, and Temkin models [22].

Table 2. The adsorption Isotherm Models.

Adsorption Isotherm Model	Assumption	Linear Expression	Parameter
Langmuir Model	All the active adsorptive sites possess equivalent binding energy and a single adsorbate can only bind with one active site at a time. Suitable for monolayer adsorbent	$\frac{C_e}{q_e} = \frac{1}{q_m K_L} + \frac{Ce}{q_m}$	q_e is the adsorption capacity (mg/g) at equilibrium; C_e is the adsorbate's equilibrium concentration (mg/L); q_m is the monolayer adsorption capacity (mg/g), K_L is the adsorption equilibrium constant (L/mg).
Freundlich Model	This model better describes the non-ideal adsorption systems and provides insights on the exponential distribution on active surface sites. Suitable for multilayer adsorption	$\ln(q_e) = \left(\frac{1}{n}\right) \ln(C_e) + \ln\left(K_f\right)$	q_e is the adsorption equilibrium capacity of the adsorbent (mg/g); n is the Freundlich constant; K_f is the Freundlich constant and C_e is the adsorbate equilibrium concentration (mg/L)
Sips Model	An hybrid of the Freundlich and the Langmuir isotherms. It adequately reduces to the Freundlich adsorption behaviour and effectively predicts monolayer adsorption system by Langmuir mode at high concentrations of the adsorbate	$q_e = \frac{(K_S C_e)\ n_S(q_m)}{1+(K_S C_e)}$	q_e is the adsorption equilibrium capacity (mg/g); C_e is the adsorption equilibrium concentration (mg/L); q_m is the Sips adsorption capacity (mg/g); K_S is the Langmuir adsorption equilibrium constant (L/mg); n_S is related to Freundlich heterogeneity factor (n_F) [$n_S = 1n_F$].
Dubinin-Radushkevich Model	The model account for the porous structure effects of theadsorbents. It is grounded on the adsorption potential theory and supposes that the adsorption was achieved through micropore space-filling, instead of layer-by-layer adsorption on pore surfaces.	$q_e = q_{max}$ X $\exp(-\beta\varepsilon^2)$	q_e is the equilibrium adsorption capacity (mg/g); $q_{\max}$ is the maximum adsorption capacity, β is the constant related to the adsorption energy (mol2/kJ-2), ε—adsorption potential (kJ/mol)
Temkin Model	The adsorption is non-uniform and active sites possess non-uniform adsorptive energies. The adsorption heat depreciates with the coverage due to adsorbate/adsorbent interaction.	$q_e = \frac{RT}{b_T} \ln(K_T C_B)$	K_T is the Temkin isotherm constant (L/g); R is the ideal gas constant (8.314 J/mol K), T is the temperature (K), b_T is a constant related to the adsorption heat (J/mol), C_e is the equilibrium concentration of adsorbate in solution (mg/L)
Redlich-Peterson Model	An hybrid of Langmuir and Freundlich isotherm model	$q_e = \frac{(K_R C_e)}{1+(a_R\ C_e^g)}$	K_R (L/g) and a_R (L/mg) are R-P isotherm constants; g is the exponent lying between 0 and 1. The limiting cases are Henry's law for g = 0 and Langmuir's form for g = 1.

3.2. Adsorption Kinetic Model

These models describe the relationship between the adsorbed adsorbate amount (q_t) and the contact time (t). Due to the occurrence of chemical reactions, kinetic prediction is vital for the adsorption system design and determination of the reaction rate-controlling step. Additionally, the adsorption nature depends on the physicochemical characterization

of the adsorbent and reaction conditions such as temperature, pH, dosage, and ionic strength. These models include pseudo-first-order, pseudo-second-order, Elovich, and intraparticle diffusion models.

3.2.1. Pseudo-First-order Model

The model describes the adsorption of liquid-solid state systems based on the adsorption capacity. The Pseudo-first-order model supposes that a single adsorbate is adsorbed onto a single active adsorptive site [23]. The linear expression is as follows:

$$\log(qe\ - q_t) = \log(q_e) - (\frac{k_1}{2.303}) \quad (1)$$

where q_e—adsorption capacity at equilibrium (mg/g), q_t—adsorption capacity at time t (mg/g), k_1—rate constant of pseudo-first-order adsorption (1/min)

3.2.2. Pseudo-Second-Order Model

This kinetic model describes the adsorption based on the adsorption capacity of the solid phases. It is commonly used for chemisorption kinetic rates. The equation for this model is:

$$\frac{t}{q_t} = \frac{1}{k_2 q_e^2} + \frac{t}{q_e} \quad (2)$$

where k_1—rate constant of pseudo-second-order adsorption (g/mg·min)

3.2.3. Intraparticle Diffusion Model

The drawback of the pseudo-first and pseudo-second-order models is that they cannot consider the diffusion and rate-controlling steps in the adsorbate molecule transportation [24]. Consequently, the intraparticle diffusion kinetic model was introduced to overcome the limitation. The equation can be written as follows:

$$q_t = k_p t^{\frac{1}{2}} + C \quad (3)$$

where k_p—intraparticle diffusion rate constant (mg/g $\text{min}^{1/2}$), C—intercept of the intraparticle model plot. To recognize that the intraparticle diffusion has been obeyed, the plot should be linear, and only if the lines pass through the point of origin is intraparticle diffusion considered the rate-controlling step. But when the plot fails to pass through the origin, the implication is that intraparticle diffusion may not be the only rate-limiting step. Other kinetic models may be responsible for controlling the adsorption rate due to their input to the net transport of the adsorbate ions.

3.2.4. Elovich Model

This model has been reported as compatible with describing the adsorption system when the adsorbate species and the adsorbent sites interact chemically via a second-order mechanism [25]. Representation of the linear equation of the Elovich kinetic model is as follows:

$$q_t = \frac{1}{\beta} \ln(1 + t\beta\alpha) \quad (4)$$

where q_t (mg/g) is the adsorbed adsorbate amount at time t, α is the initial rate constant (mg/g·min), and β is the desorption constant (g/mg).

4. Materials for Adsorption of Toxic Materials in Wastewater

Adsorptive materials are classified into two main groups, conventional and nanostructured materials, and their difference is seen in their sizes, shapes, and removal capacities toward water pollutants [26]. As a result, the current review will be on the selected and frequently used adsorbents for efficient toxic metal uptake.

These adsorbents are the usual types for wastewater remediation [27]. They are naturally available and can be easily derived from waste materials or applied in their pristine form [13]. These adsorbents are activated carbons, zeolites, industrial solid waste, biomaterials, and clay minerals. Conventional adsorption materials are costly, a significant limitation to their industrial application. Consequently, non-conventional adsorbents are products and by-products of biological (algae, bacteria, fungi, and yeasts), industrial (red mud, sludge), agricultural materials (cellulose, starch, and chitosan, bark, sawdust, peat) as well as nanoparticles are increasingly becoming popular. The non-conventional materials have advantages as adsorbents because of their abundance and attractive physicochemical characteristics [28].

4.1. Activated Carbons

Activated carbons (ACs) are commonly used as adsorbents in aqueous media due to their porous surface (large micropore and mesopore), improved specific surface area, as well as various compositional groups which bound to graphite-like layered edges [29,30]. The ACs' adsorption behavior depends on the functional groups, pore size, and distribution [5,13]. Some carbonaceous precursors used to synthesize ACs are biological, fruit, plastic, agricultural, and vegetable wastes [5,31]. The materials are well known for retaining particular compounds and the preferential characteristic of resultant high-performance adsorption [32,33]. Due to the capital expenditure on coal-derived ACs, various agricultural wastes have been used for ACs synthesis. Invariably, there is a resultant positive impact on industrial and agricultural wastes in terms of reduced cost

There are numerous physical and chemical activation agents used for AC production. Some chemical activating agents are KOH, $ZnCl_2$, H_3PO_4, and physical activations are steam atmosphere, air, and CO_2 [30].

4.1.1. Chemical Activation Method

The method is based on a single-step reaction involving impregnating suitable reagents into the raw carbon source. Some activation agents include alkali metal-based salts and acids/bases (HCl, HNO_3, H_3PO_4, H_2SO_4, NaOH, KOH) [34]. In this method, the enhanced surface area of ACs (>3000 m^2/g) under low employed temperature can be achieved compared to physically modified ACs. The activated carbon has been produced from the flower of the golden shower tree through chemical activation, which yielded a large surface area of 1413 m^2/g [35]. The method's advantages are scalability, good pore growth, and less energy and consumption. However, the purification process may not be trivial for residual impurity removal. The method may use corrosive and hazardous chemicals, which could threaten waste disposal [36]. KOH chemically activated the Eichhornia (water hyacinth) with surface area (900 m^2/g) and average pore diameter (21.6 Å) [37]. The adsorption data followed Freundlich and pseudo-second-order models with adsorption of Cd and Pb as 49.5 and 102 mg/g. The optimum adsorption was achieved at pH = 7, adsorbent dose (50 mg) at a temperature of 30 °C. The teak sawdust was also used to produce AC by hydrothermal/chemical activation using $ZnCl_2$. The adsorption capacities achieved were 208 and 182 mg/g for Cd and Cu by the Langmuir model. Further exploration was that the oxygen functional groups readily accounted for pronounced adsorption output and the complexation mechanism was superior to the electrostatic interaction. The Eucalyptus camaldulensis was chemically activated by H_2SO_4 to remove Cd, Pb, and Cr from the wastewater through adsorption batch experiments [38]. The data obey the Langmuir model with adsorption capacities of 47.62, 6.17, and 9.26 mg/L for Cr, Cd, and Pb (with basic solution (pH 10–12)), thus suggesting a monolayer coverage adsorption system.

4.1.2. Physical Activation Method

This method involves pyrolysis, which majorly occurs at high temperatures. Generally, the process involves two main steps (carbonization of carbon materials in an inert atmosphere and, lastly, the resultant material activation in the presence of gasification

reactants like steam atmosphere, air, CO_2, and their mixture). The activation temperatures are typically in the range of 700–1100 °C. The reaction between the water and the gas can be assembled as follows:

$$C + H_2O \rightarrow CO + H_2 \quad (5)$$

$$C + 2H_2O \rightarrow CO_2 + 2H_2 \quad (6)$$

The carbon is gasified, and porous, highly activated carbon is produced.

This process involves two steps: carbonization of carbonaceous materials in an inert atmosphere and activating the resulting materials in carbon gasification agents such as stream, air, and carbon dioxide. The sewage sludge was activated through heating at 800 °C for effective removal of Cu, Cd, and Pb from the wastewater, and the optimum removal parameters were pH = 6, room temperature, for 60 min, and that afforded the Freundlich (for Cd, Pb), and Langmuir (Cu) with a removal efficiency of 99.5, 97.7 and 93.7%, respectively [39]. The Ulva Lactuca was also activated at 800 °C for 3 h for batch adsorption of Cu, Cr, Cd, and Pb with 84.7, 82, 84.6, and 83.3 mg/g at pH 5 and equilibrium time (1 h) using Langmuir model, respectively [40]. The merits of the method are avoiding impurities typically sourced from an activating agent, inexpensive, no need for post-synthesis purification, and non-corrosive procedure. In contrast, the possible demerits are longer synthesis time, high pressure and temperature use, and weak control of porosity [41].

4.2. Zeolites

They are defined as 3D crystalline alumina silicates sourced from the interlinked tetrahedral arrangement of silica (SiO_4) and alumina (AlO_4) moieties [26,30]. The attributes of the tetrahedral zeolites framework are reversible dehydration and ion exchange. Zeolites have industrial and scientific importance due to their large surface area, improved ion exchange properties, inexpensive hydrophilic characteristics, and abundance, which result in their suitability for efficient toxic metals uptake from wastewater effluents [42,43]. These materials can occur naturally and also be synthesized [44,45]. The most abundant natural zeolite is clinoptilolites for effectively removing the metal species. However, they suffer the good pore size and impurity presence [44]. As a result, the synthetic counterparts exhibit even better adsorptive behavior and affinity for metallic adsorbates [46,47]. The zeolite preparation can also be achieved via sol-gel, hydrothermal, and microwave methods, which are presented and briefly discussed in this review.

Sol-gel synthesized faujasite X zeolite was studied for removal of several metals and examination of multiple adsorption parameters resulting in efficiency greater than 70% for metal and followed the order Zn > Cu > Pb > Fe from the municipal wastewater [48]. The hydrothermally derived incinerator ash zeolite was applied for the removal test of Cd, Cr, and Pb batch mode [49]. The modified zeolite afforded higher removal efficiency (84, 99, and 78% for Cr, Cd, Pb) than the natural zeolite in industrial wastewater and simulated metal solution samples under optimized conditions (60 min. and 1 mg of adsorbent). In the order study, the sol-gel assisted calcination method was used to prepare Faujasite for uptake of Pb, Zn, Cu, Cd, Fe, and Cr from industrial wastewater with an efficient range of 19.27–86.47% [50]. The tested equilibrium data and kinetics have followed the Langmuir model (homogenous adsorption system characteristic) and pseudo-second-order. The Na-zeolite P_1 was synthesized by NaOH treatment, and the achieved surface area was 40 m^2/g compared to raw pumice (31 m^2/g). The pore volume of Na-zeolite P_1 (0.02 cm^3/g) was two-fold of the pumice [51]. The maximum obtained efficiencies under the optimized system were Cu (76%), Cd (98%), and Fe (76%). The equilibrium was achieved within a small contact time (8 min) due to the availability of the unoccupied adsorbent's surface area, thus qualifying a faster adsorption rate. Furthermore, the high removal efficiencies may also be attributed to the adsorption mechanism and possible ion exchange occurrence [52]. The homogenous and heterogenous surface presence of Na-zeolite P_1 was evidenced by equilibrium data obeying the Langmuir and Freundlich models. In contrast, the adsorption

rate was well described by pseudo-second-order (characteristic of possible chemisorption, adsorption rate on the adsorbent surface is the responsible agent for rate controlling step).

4.3. Clay Minerals

These are types of materials readily found in nature. The clay products are hydrous aluminosilicates composed of weathered rocks, water, alumina, and silica and are well known to be 4 μm in at least 1-D [20]. Their standard features (large ratio of surface area to volume, pore volume, and small sizes) produce extraordinary catalytic and improved cation exchange capacities [7]. Moreover, the porous surface houses attractive forces suggesting the possible high bonding power [53]. The adsorptive removal of the toxic metal in wastewater via clay mineral may reasonably be achieved through complex adsorption mechanism series like direct bonding involving surface complexation, ion exchange, and direct contact uptake between clay mineral surface with cationic adsorbates [54]. The standard structural units are Al-O octahedral and Si-O tetrahedral layers bond to oxygen [55]. Based on structural arrangements and surface constituents, the clay minerals are mainly grouped into bentonite, mica, and kaolinite [56].

The bentonite is a sedimentary rock made up of a 2:1 layer clay structure and cations (Na, Ca, Mg, Fe) situated between the sheets. The tetrahedral and octahedral layers are patterned so that tetrahedral tips in each silica layer and mono-hydroxyl layer qualify as a monolayer [7].

The kaolinite clay minerals are a 1:1 layered structure composed of octahedral and tetrahedral SiO_4 layers. Moreover, the hydrogen atom accumulation with other minerals tends to constitute the clays' metal cation adsorption in an aqueous medium [57].

Lastly, the Mica group consists of a 2:1 layered structure with substitution (Si^{4+} substituted by Al^{3+}) occurring in tetrahedral sheets by clay minerals [58,59].

There are naturally found and modified clay minerals for improving porosity, surface area, and affinitive surface. These developments are commonly achieved through physical and chemical treatments, viz. acid activation, salts, bases, thermal, surfactants, and supported on polymers [60,61].

4.3.1. Thermal Treatment of Clay

The heat treatment for synthesis may transform and tune the clay crystallinity, size, shape, and amorphization of porous nature. The thermal activation process is partitioned into temperature ranges for successful synthesis. The first one is the temperature beyond the dehydration (where records have shown that minerals like kaolinites tend to change to amorphous pore shapes). The second classification of temperature ranges is temperatures between dihydroxylation (process lowers structural water and transforming micro and macro porosity) and dehydration (elimination of adsorbed waters). The third temperature entails more crystalline phase generation (starting crystallographic orientation change) [62].

The thermal treatment does not utilize multiple chemicals for clay synthesis. However, determining adequate calcination temperature for multiple clay products may be difficult and extreme conditions may also result in clay mineral structural disintegration [61].

4.3.2. Acid Activation of Clay

During the acid activation of the clay, the first step in this process involves protons intercalation between clay intersheet spaces. The following footprint consists of dissolution cations and orientation on the silicate sheet. In most cases, the acid activation is performed using acids such as hydrochloric and sulfuric acid [63]. This activation has improved acidity, porosity, and surface size for catalysis on toxic metal adsorption. The common acids utilized for activation are nitric, hydrochloric, sulfuric, and phosphoric acids [64].

4.3.3. Polymerization of Clay

Due to their exceptional physical and chemical properties, the polymerization and surfactant-assisted polymerization of clay minerals have attracted use in environmental

remediation applications. In this process, the ordering with the clay intersheet space tends to depend on the chain length, density, and applied temperature [65]. Some used polymers include polyurethanes, polyvinyl chloride, polystyrene, polyethylene terephthalate, polyimides, and polyesters [65,66].

5. Nanotechnology

Nanotechnology presents an extraordinary platform for synthesizing adsorbents with better capacity for uptaking pollutants and toxicity mitigation in wastewater [67–69]. This technology encompasses atomic material modification between 1 to 100 nanometers in size. The resultant nanomaterial has better chemical, physical, mechanical, and catalytic properties than its bulk material counterparts [61]. Due to their features which include low heat modifications, multiple active adsorption sites, tunable pore structure and size, large specific surface area, and short intraparticle diffusion length. Nanomaterials have been coupled with adsorption methods for achieving better toxic metal removal from wastewater [70]. A good adsorbent is considered a nanomaterial that is preferably non-toxic, possesses greater absorptivity, consumes less energy, is recyclable, and is reusable [71]. Amongst them are carbon-based nanomaterials, metal oxide nanoparticles, and nanocomposites. Nanomaterials are categorized as nanolayer/sheet, nanotubes, nanoparticles, nanospheres, nanowires, etc.

5.1. Metal Oxide Nanoparticle

In recent years, nanostructured metal oxide has proved to be the best candidate for wastewater treatment via an adsorption mechanism [72]. As some common characteristics associated with nanomaterial, metal oxide nanoparticles are no exception because they possess large pore volumes, surface area, high adsorption capacity, well pore sizes, and functionalized site/s [73]. Some nanosized metal oxide nanoparticles are zinc, manganese, aluminum, zirconium, iron, titanium, magnesium, etc.

5.1.1. Iron Oxide-Based Nanoparticles

The fourth abundant element in Earth's crust is iron. The availability and ease of fabricating iron oxides have resulted in extensive studies on these nanomaterials. They have better adsorption capacity, affinity, and quicker adsorption rate than other adsorbing materials. Iron nanomaterials are readily used for toxic metal adsorption from water and wastewater. Iron-based nanomaterials may be classified into maghemite (γ-Fe_2O_3), goethite (α-FeOOH), magnetite (Fe_3O_4), hydrous ferric oxides (HFO), and hematite (α-Fe_2O_3). The most commonly used iron forms are α-Fe_2O_3, Fe_3O_4, and γ-Fe_2O_3 due to chemical stability, magnetism, less toxicity, and large surface area [74].

Magnetite (Fe_3O_4)

The cubic ferromagnetic magnetite is efficiently used for metallic pollutants adsorption due to its magnetic property, enabling simple separation and regeneration of the adsorbent from the aqueous solution [75]. Multiple investigations for removing toxic metals have been performed and documented [76]. The smaller the magnetite size (decreased ionic radii), the faster the metal ion diffusion to adsorbing surfaces of the adsorbent [77]. The magnetite nanoparticles were synthesized via co-precipitation, (surface area: 94.43 m^2/g, pore size: 2–60 nm, pore volume: 0.02–0.35 $cm^3/g/Å$) [78]. Simultaneous adsorption of Cd(II), Cu(II), and Pb(II) was performed on river water samples using porous Fe_3O_4 nanoparticles. The reported mixed removal efficiency of Cd(II), Cu(II), and Pb(II) was 80, 84, and 86% [79]. Furthermore, equilibrium data were best fitted by the Langmuir isotherm and pseudo-second-order rate model. In this case, the Langmuir isotherm proves that all active adsorption sites are uniformly distributed on the magnetite adsorbent, and the adsorbates occupy adsorption sites on the adsorbent resulting in a monolayer adsorption system. The pseudo-second-order indicates that the adsorption rate on the adsorbent

surface is the rate-controlling step [77,78]. Several studies have been conducted for metal ions elimination using Fe_3O_4 adsorbent [77].

Hematite (α-Fe_2O_3)

The rhombohedral, hexagonal, weakly ferromagnetic hematite nanoparticles are considered the highly stable form of iron oxide, which also exhibits anti-corrosive properties and has been used in energy and catalytic functionalities [80–82]. These nanoparticles have been applied in wastewater treatment for metal removal [83]. The applicability of hematite nanoparticles prepared through co-precipitation was investigated for removing Cd and Pb from the wastewater [70]. The synthesized adsorbent had an average particle size (40 nm) and BET surface area (39.18 m^2/g). Various operating factors involving contact time, pH, and metal ion initial concentration were studied. The adsorption experiments informed that the maximum adsorption capacity of α-Fe_2O_3 associated with Pb(II) and Cd(II) was found to be 20 and 11.63 mg/g under optimized conditions (time: 10 min., pH 7, dosage: 0.15 g, at room temperature). Moreover, the adsorbent had an affinity towards Pb(II) than Cd(II) uptake, and the equilibrium adsorption data best fitted Langmuir than the Freundlich isotherm model [70]. In another study, the hematite was tested for adsorption of Zn (II), Cd (II), Pb (II), and Cu (II) with affinitive order: Pb (II) > Zn (II) > Cd (II) > Cu (II) and the adsorption best-fitted pseudo-second-order model [84].

Maghemite (γ-Fe_2O_3)

Similar to magnetite, tetrahedral maghemite possesses ferrimagnetic characteristics and a large surface area which serves as better adsorptive agent properties for treating toxic metals from wastewater treatment [85]. The ease of synthesis and process-ability of the nanoparticles makes them widely investigated. However, the increased synthesis temperature tends to convert the maghemite into hematite, thus causing the loss of maghemite magnetism [86]. The synthesized maghemite nanoparticles were tested for removal of Cu, Cd, and Cr from wastewater through batch experiments, and adsorption parameters were also studied. The findings revealed that the adsorption readily depended on the pH (6–10) and obeyed the Langmuir isotherm model [87].

5.2. Titanium Oxide-Based Nanoparticles

The TiO_2 nanoparticles possess simple synthesis, photocatalytic, inexpensiveness, and chemical stability, which is a potential candidate for removing toxic metals from wastewater and artificial aqueous solutions. The commonly used phase compositions are rutile and anatase, which are essential for industrial use, unlike brookite [87]. Remarkable Cd, Cu, and Pb removal from aqueous solutions using TiO_2 nanoparticles were performed through batch experiments [86]. The equilibrium data for all the single and mixed ion solutions followed Freundlich and the first-order model. The adsorption capacities with precipitation synthesized TiO_2 nanoparticles (size = 10 nm) were evaluated as 120.1, 50.2, 39.3, and 21.7 mg g^{-1} for Cd, Cu, and Pb [88]. In other study, TiO_2 resulted in successful adsorption of Cd (removal efficiency ~100% and adsorption capacity = 101.1 mg/g) in wastewater at starting concentration 25 mg/mL, NPs dosage (0.64 mg/mL), pH = 7 and contact time = 72 h. The adsorption correlated well with the pseudo-second-order kinetic rate model (R^2 = 0.918) and Freundlich isotherm model (R^2 = 0.994). The removal rate of adsorbate on the adsorbent surface was the rate-determining step, and Freundlich readily observed the heterogeneous adsorption system.

5.3. Zinc Oxide-Based Nanoparticles

Due to improved surface area, mechanical and thermal stability under room temperature, and better removal capacity, the ZnO nanoparticle has been effectively applied for metal pollutants removal from the water and wastewater [89]. Besides the use in wastewater purification studies, the electrochemical coupling coefficient, high chemical stability, wide radiation absorption range, and pyroelectric and piezoelectric properties of these

materials have made the nanoparticles promising in catalysis, solar cells, capacitors, gas sensors, drug delivery studies [90]. Further merits associated with ZnO nanoparticles are simple and cheaper synthesis and tunable morphological properties. As a result, several methods (electrochemical, solvothermal, microwave, hydrothermal, and vapor deposition methods have been adopted for the fabrication process of the nanoscaled ZnO particles. To date, various zinc precursors like ($ZnCl_2$), ($Zn(NO_3)_2 \cdot 6H_2O$), ($Zn(SO_4)_2 \cdot 7H_2O$), and ($Zn(C_2H_3O_2)_2 \cdot 2H_2O$) have been employed for ZnO nanoparticles fabrication. Most importantly, synthesizing ZnO in a medium below pH = 7 (low OH^- concentration) results in the hindrance of hydrolysis and condensation, which may, in turn, lead to weaker crystallization and aggregates formation. In the case of a neutral medium (pH = 7), due to equal concentrations of the OH^- and H^+, the solution mixture may exhibit small or no intensive contribution at ZnO crystal interfaces [91]. The advantageous pH for the growth of ZnO nanoparticles is preferably above seven due to a greater concentration of OH^- which electrostatically attract incoming positively charged Zn^+ ion, which could uplift small ZnO nanoparticle and crystallization [92]. Additionally, the incubation time, precursor and surfactant concentrations, and calcination temperature affect the nanoparticle's surface area, morphology, size, and phase composition of the synthesized ZnO nanoparticles.

ZnO nanoparticles have been fabricated using Centaurea cyanus extract (biosynthesis) at ambient temperature, and the average particle size was 49 nm [82]. The optimum adsorption conditions were adsorption time = 91.25 min., adsorbent dosage = 1.63 g/L, Pb initial concentration = 77.5 mg/L, pH = 5.5, and removal efficiency = 99.24%. The equilibrium adsorption data obeyed pseudo-second-order and Freundlich isotherm, implying that the active and available adsorption sites were heterogeneously dispersed on the ZnO nanoparticle surface and subsequent adsorbate coverage resulted in a multilayer adsorption system. The batch experiments were performed for Co, Cd, and Pd using casein-capped ZnO nanoparticles (size = 10 nm) [93]. The pseudo second rate order and Langmuir isotherm model have been obeyed, and subsequent adsorption capacities for Pd, Co, and Cd were 194.93, 156.74, and 67.93 mg/g, respectively.

6. Carbon Nanomaterials

Due to carbon's exceptional electrical, mechanical, and thermal properties, its nanomaterials have been good candidates in electronics, drug delivery, etc. [94]. Furthermore, features such as ease of functionalization, high sorption capacities, large surface area, non-toxicity, and affinitive behavior have made carbon material suitable for organic, pathogenic, and inorganic contaminants removal from wastewater bodies [95]. Carbon nanomaterials have been widely used to remove heavy metals due to their high sorption capacities and non-toxicity.

Graphene Nanomaterials

Graphene is one atom thick, 2D atomic crystal sp^2 hybridized carbon allotrope material with a single layer, Bernal, hexagonal, or rhombohedral stacked arrangement with partially occupied π orbitals occurring below and on top of the graphene plane and exhibiting extraordinary properties, like stiffness, elasticity, electrical, thermal conductivity, surface reactivity, and mechanical strength which also make the graphene-based nanomaterial to be applied in wastewater remediation [96]. Additionally, the graphene properties depend on the defect's density, sheets thickness, and count. The graphene material can be partitioned into three, namely: pristine graphene (pG), graphene oxide (GO), and reduced graphene oxide (rGO). Through oxidation of pG, the GO has been formed with various oxygen functional groups (carboxyl, carbonyl, epoxide, hydroxyl), whereas the rGO is the reduced form of the GO. Among these materials, pG has been documented as a structural defect-free crystal [83]. However, the high negative charge density and hydrophilic nature of the rGO and GO favor metal cation uptake for wastewater treatment [97]. The functionalized pG, GO, and rGO presents extraordinary selectivity, affinity, removal capacities, and efficiencies in treating metal-contaminated wastewater [98].

Due to the unique properties of graphene (Table 3), these nanostructures have gained a vast application range, including energy cells, advanced composites, diffusion barriers, protective overcoats, biosensors, supercapacitors, membrane technology, and semiconductors.

Table 3. Chemical and physical properties of graphene.

Material	Property	Magnitude	Material Comparison
Graphene	Thermal conductivity	5×10^3 W/Mk	10 × greater than Cu
	Young's modulus	1.1 TPa	-
	Electron mobility	2×10^5 cm^2/Vs	140 × greater than Si
	Radiation transmittance	97.7%	Alternative to fluorine-doped tin oxide (FTO) and indium-tin oxide (ITO)
	Tensile strength	125 GPa	Specific strength 100 × higher than steel
	Permeability	Impermeable towards gas/liquids; permeable to protons	Pore size is smaller than H_2, and He diameter
	Surface area	2630 m^2/g	2 × larger than carbon nanotubes (CNTs)

7. Synthesis of Metal Oxide Nanoparticles

Various chemical, physical and biological methods have been employed for the synthesis of metal oxide nanoparticles [99]. They can be categorized into bottom-up (biological and chemical processes) and top-down (physical methods) [100]. The top-down or destructive approach involves decomposing bulk material into smaller units, followed by conversion to desired nanoscaled particles [101]. The approach comprises various decomposition methods like physical vapor deposition, grinding, pulsed laser ablation, and ball milling. In a bottom-up or constructive approach, the atoms or small molecular precursors are built up to form nanoparticles after the nucleation process. Electrospinning, sol-gel, hydrothermal, microemulsion, co-precipitation, electrochemical, thermal decomposition, and biological methods are bottom-up approaches.

The commonly used methods for TiO_2, Fe_3O_4, ZnO based nanoparticles are sol-gel, micro-emulsion, electrochemical method, thermal decomposition, biological synthesis, and several other procedures. Despite the utilization of several methods used for nanoparticle fabrication, co-precipitation is the more effective, more practical, cheap, and most universal method for nanoparticle growth [102]. Thorough tuning of pH, precursor-co-precipitant ratio, temperature, and agitation rate may readily result in well-shaped, sized, phased, and scalable nanoparticles. TiO_2, Fe_3O_4, and ZnO particles have extensively used toxic metal (Cu, Zn, Cr, Cd, Fe, Pb) adsorption from simulated wastewater [103]. The metal oxide nanoparticle's uptake efficiency is highly dependent on a surface charge, size, surface area, catalytic strength, available adsorption points, and the shape of the adsorbent [104–106]. Similarly, these findings have been almost consistent with the synthesized adsorptive nanoparticles for wastewater remediation [93]. Since the metal oxide property change is highly dependent on synthetic steps, there are advantages, influencing aspects, merit, and demerit associated with the method, as summarized in Tables 4 and 5.

Table 4. Various methods are employed for the synthesis of metal oxide nanoparticles.

Method	Highlight	Influencing Factor	Merit	Demerit
Hydrothermal	The reaction is performed in an autoclave or reactor in an aqueous media at a pressure beyond the solvent boiling point and high temperature	Incubation time, temperature, precursor concentration, reactants ratio	Structural shape and size are tunable. Capable of producing impurity-free nanomaterial since it is a closed system reaction	High energy consumption. High-pressure use

Table 4. *Cont.*

Method	Highlight	Influencing Factor	Merit	Demerit
Co-precipitation	The reaction of precursor salt in an aqueous solution to a base with a mild oxidant.	Highly dependent on reagent ratio use, stirring rate, pH, and temperature	Highly scalable. Relatively narrow size distribution. Less reaction period. Simplicity and can be performed under ambient conditions	Possible agglomeration. May result in impurity formation. High pH use during the synthesis and purification. Not suitable for precise stoichiometric phase fabrication.
Micro-emulsion	Water immersed in an oil medium, then stabilized molecular surface medium followed by elimination of surfactant and particle purification	Salt type, pH, type of surfactant consumed	Fairly low-temperature use (20–80 °C). Time-consuming method (roughly to hours). Better shape control.	Processability may be complex—low yield of colloids.
Biosynthesis	Biomaterials are used as reducing agents to yield particles from the appropriate precursors	Precursor-biomaterial mole ratio, temperature, incubation time, pH, agitation rate	Achievable under room temperature. Reduced toxic chemical use.	May be complex to support reproducibility. Low production yield. Time-consuming. Inadequate nanoparticle shape control.
Sonochemical	Applying high-power ultrasound radiation initiates a chemical reaction by generating acoustic cavitation.	Temperature, pressure, heating and cooling rates, frequency	Low-temperature use (18–50 °C). Simple and can be performed under ambient conditions. Less time consumption	Bad shape tuning. Non-trivial for large-scale nanoparticle production.
Vapor methods	The vapor composition is made unstable relative to the generation of resultant particles	Temperature, atmosphere, precursor, synthesis time, evaporation-condensation rate	Reasonable synthesis time (minutes–hours). Highly scalable. Fair shape control. Good material purity	Not simple to perform. High-temperature consumption.
Electrochemical deposition	The occurrence of deposition is at the electrolyte interface housing the metal to be deposited along with the conductive metal substrate	Applied potential, electrode nature, residence electrolyte chemical nature, metal substrate	Eco-friendly (less chemical consumption). Readily performed under room temperature. Fair shape control.	Expensive instrumentation. May suffer yield control—limited electroactive electrode use.
Thermal decomposition	The disintegration of bulk material into nano/finer particles via the high-temperature application	The atmosphere used, temperature, heating rate	Highly scalable. Good shape tuning. The capability of producing contaminant-free particles.	May be complex to use. High-temperature use. May induce structural disintegration
Sol-gel	It comprised of hydroxylation and precursor condensation followed by solvent removal or gelling by reaction	Precursor concentration, temperature, gel nature, pH, stirring rate, reaction kinetics	Wide reaction temperature use including room temperature (25–200 °C).	Medium yield. Better shape tuning. The reaction may span hours for quality colloid production

Table 5. The synthesized metal oxide nanoparticles are applied for the adsorptive removal of metal ions in an aqueous solution.

Adsorbing Material	Preparation Method	Surface Area (m^2/g)	Size (nm)	Adsorbed Metal	Conditions	Kinetic Model	Isotherm Model	Removal Capacity (mg/g) Or Efficiency (%)
α-Fe_2O_3	Co-precipitation	24.82	75	Cu	25 °C, pH = 5.2, 225 min	pseudo-second-order model	Langmuir	84.46 mg/g
γ-Fe_2O_3	Sol-gel	198	10	Cr, Cu	25 °C, pH = 2.5 (Cr), 6.5 (Cu), 10 min	pseudo-second-order model	Langmuir isotherm	17.0 mg/g (Cr), 26.8 mg/g (Cu)
	Co-precipitation	NA	14	Cr, Cu, Cd	70 °C, pH = 10 (Cd), 6.5 (Cu), 2.6(Cr), 10 min	NA	Langmuir model	8.4% (Cd), 84.4% (Cr), 88.2% (Cu)
α-FeOOH	Co-precipitation	71.49	15	Cu	25 °C, pH = 5.2, 225 min.	pseudo-second-order	Langmuir model	149.25 mg/g
Fe_3O_4	Co-precipitation	-	8	Pb, Cu, Zn	25 °C, pH = 5.5, 24 hr.	pseudo-second-order model	Langmuir model	41.76 mg/g (Zn), 43.21 mg/g (Cu), 149.18 mg/g (Pb)
Fe_3O_4	Co-precipitation	-	<10	Pb, Cu, Zn	25 °C, pH = 5.5, 6 & 6.5, 120 min	pseudo-second-order, Elovich model	Langmuir model	Pb—(90%), Cu—(40%), Zn—(30%)
Fe_3O_4	Solvothermal	11.3	45	Pb, Cr	25 °C, pH = 5 & 6, 48 h	pseudo-second-order	Langmuir	19 mg/g (Pb), 9 mg/g (Cr)
TiO_2	Degassing and thermal treatment	185.5	8.3	Pb, Cd	25 °C, pH = 8, 120 min	-	Langmuir	401.14 mg/g (Pb), 135.14 mg/g (Cd)
TiO_2	Co-precipitation	208	50	Zn, Cd	25 °C, pH = 9, 30 min.	-	-	15.3 mg/g-(Zn), 7.9 mg/g-(Cd)
TiO_2	Co-precipitation	-	15	Cu	25 °C, pH = 9, 30 min.	-	Langmuir	Cu—(97.72%)
ZnO	Green synthesis	-	10 ± 2.6	Pb	70 °C, pH = 5, 60 min.	pseudo-second-order model	Langmuir model	19.65 mg/g, 93% (Pb)
ZnO	Co-precipitation	15.75	25	Cr	50 °C, pH = 2, 120 min	pseudo-second-order	Freundlich	95%
ZnO	Green synthesis	701.88	10	Cd, Pb	30 °C, pH = 7, 30 min	pseudo-second-order	Langmuir	Cd—(156.74), Pb—(194.93), ~ 90%
ZnO	Sol-gel	8.25	46.5	Cd	25 °C, pH = 7, 12 hr.	pseudo-second-order	Langmuir	214.4 mg/g
ZnO	Co-precipitation	-	24.7	Cu	69.85 °C, pH = 4, 120 min.	pseudo-first-order	Freundlich	226 mg/g

The synthesis of graphene is grouped into two main method categories, i.e., the direct and indirect methods (Figure 1). In the direct methods, the graphene is directly developed on the substrate surface via the steps that utilize a solid carbon mother source. The indirect procedures involve depositing carbon sheets on the substrate surface, followed by conversion to graphene through the energy post-treatment process.

Various methods for graphene synthesis have been established, such as liquid-phase exfoliation, mechanical exfoliation and cleavage, thermal decomposition, electrochemical process, oxidation/reduction, and a few other procedures [107,108]. The synthesis method and carbon source type constitute various categories for graphene synthesis. Graphene may be surfaced on the single-crystal transition metal via laser ablation, chemical vapor deposition (CVD), spin coating, and physical vapor deposition (PVD). The PVD is preferred over CVD due to the achievement of low-temperature use, high yield, and manageable graphene growth on multiple substrate surfaces. In contrast, the CVD method is reported to have sensitive deposition conditions such as growth time, gas concentration, substrate surface, and temperature [109].

The PVD of graphene may be accomplished via ion plating, sputtering, ion beam-assisted growth, and vacuum evaporation [109]. Furthermore, the PVD graphene synthesis can be achieved through direct (growth by utilizing significant energy carbon source and the transitional metallic substrate) and indirect method (deposition through energetic post-growth treatment for amorphous carbon film conversion to graphene structure).

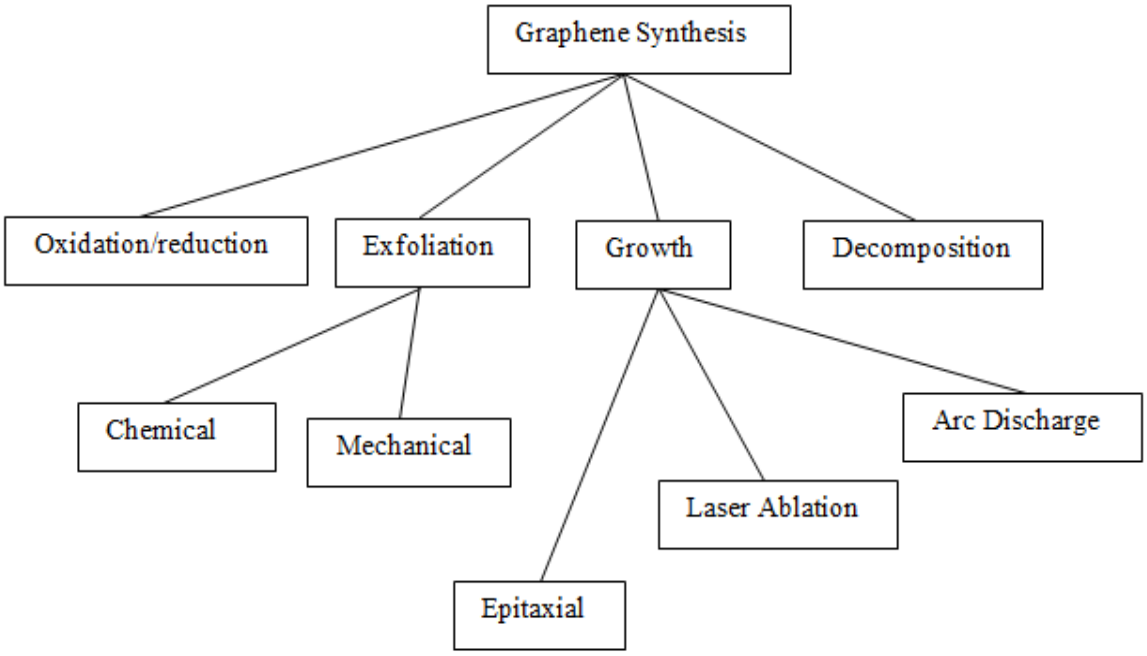

Figure 1. Methods for the synthesis of graphene.

Direct graphene growth involves high-temperature vacuum evaporation of graphite through high-energy treatment. This results in the controlled growth on transitional metal or alloy substrate surface connected to the process chamber cathode. The method set includes arc discharge, laser, unzipping carbon nanotubes, etching, and chemical and mechanical exfoliation [109]. In these methods, the carbon source may be fullerene, graphite, amorphous carbon film, and carbon nanotubes. The evaporation potential can be sourced from ablation, arc discharge, and pulsed laser deposition [110]. However, modeling the deposition conditions for graphene fabrication may be moderately hard and more significant.

The fabrication of graphene is achieved from liquid, gaseous, and carbonaceous precursors. Furthermore, the method involves atom/molecule decomposition from suitable precursors followed by an in-situ arrangement to generate the hexagonal graphene structural sheet/s [111]. Some methods are epitaxial growth, chemical vapor deposition (CVD), and pyrolysis. It is documented that crystallized amorphous carbon (possibly in-housing small impurities and crystal defects) exhibits thermodynamical instability compared to the graphite carbon source ($\Delta G < 0$ for amorphous carbon to graphite change and kinetically stable resulting in slow transformation-to-graphene rate). Due to the atomic structuring in both 2D and 3D irregular and multiple bonded structures, a phase transformation initialized from amorphous to crystallized carbon needs high temperature and pressure. The challenge is that a small amorphous carbon fraction may be converted into graphite. As a result, the transitional metal substrate has been put in place for graphene deposition via low pressure and temperature use [112].

7.1. Direct methods

7.1.1. Arc Discharge

This is accomplished by passing a direct current between high purity graphite electrode pair on the inert gas environment at ~500 torr and has been employed for the fabrication of carbon nanomaterials (e.g., carbon nanotubes (CNTs), graphene, fullerenes (C_{60})), metal/metal oxide nanoparticles [113]. The inexpensive synthesis of a few sheets of graphene has been achieved through this method aided by multiple uses of buffer gases (such as hydrogen (H_2), argon (Ar), and helium (He)) which help in bond breakage existing between the carbon layers, resulting into combatting the graphitic layer closing and roll up

condition. Additionally, the mixed H_2/He treatment's merit helped yield a large surface area and high crystalline graphene [114]. However, the limitation associated with the method is the use of high pressure/chamber temperature, which may suffer stacked and aggregated graphene products [115].

7.1.2. Laser Procedures

The techniques used in graphene synthesis through laser methods are pulsed laser deposition and laser ablation. The laser exfoliation may be employed to catalyze halogen removal from the graphene surface, followed by a detachment of the graphene sheet portion [109]. The carbon materials are generated on the irradiated graphitic surface during the laser ablation. Ultraviolet light may be used for peeling and direct deposition of graphene nanolayer/s onto the substrate with no need for catalyst use. Furthermore, the graphene synthesis may be achieved under room conditions, but in most cases tuning of processing parameters (applied pressure, focal length, substrate distance, laser ablation volume, and energy) may be fairly complex but more significant for graphene synthesis [116].

7.1.3. Pulsed Laser Method

Pulsed laser deposition (PLD) is one of the physical vapor deposition methods for graphene growth by graphite target irradiation in a vacuum using the transitional metal substrate [117]. The process involves direct graphene growth on the substrate at high temperatures without the carbide generation at the metal-graphene face. Multiple steps involved during graphene growth are carbon atom adsorption, precipitation, segregation, recrystallization, and these processes occur because of transitional metal and carbon atom interaction [118]. The parameters influencing the graphene growth quality, such as thickness and layer number, are laser wavelength, fluence, pulse duration, and repetition rate. Secondly, the background pressure, vacuum level, substrate distance, and temperature are influential parameters during the synthesis [119]. In this method, the laser is situated outside of the vacuum, thus enabling the synthesis under ambient conditions, and using an ultrahigh vacuum. The advantages of the PLD method are better adhesion to the substrate, low processing temperature, and reasonable growth rate.

7.1.4. Reduction of Graphene Oxide

The preparation of a large yield of few-layer graphene has been achieved through graphene oxide reduction [120]. In a specific procedure, the graphite oxide has been synthesized through oxidative treatment of graphite by using oxidants such as nitric acid, potassium permanganate, and sulfuric acid, commonly through the simple Hummers method. This process is followed by the reduction phase whereby reducing agents such as pyrrole, hydroxylamine, ascorbic acid, phenylhydrazine, hydroquinone, glucose, and sodium borohydride have been used to reduce the oxygen content of the graphene oxide and thus, successful reduction leading to few-layer pristine graphene [121]. The restoration of graphene's unique sp^2 hybridized property is also enhanced by H_2 addition, which takes place across the alkenes, calcination under nitrogen/argon gas. The method is time-consuming, requires thorough washing, and uses strong oxidizing and reducing chemicals.

7.1.5. Mechanical Exfoliation

The method involves the transference of kinetic potential to the bulk material, resulting in micro-size and nanoscaled size generation. Several studies on graphene fabrication using mechanical exfoliation for achieving a series of graphene thickness, surface area, thermal properties, and others have been documented using highly ordered pyrolytic graphite, natural graphite, and monocrystal graphite [120,122]. Some literature refers to micromechanical cleavage as a scotch tape procedure. This is well known since the graphene sheet's bonding strength to an adhesive tape was employed to counteract the effect of the weak van de Waals forces in graphite molecule. Cutting the graphite (carbon source) into mono-to-few sheets can be achieved via both room and high temperatures. However,

the method requires an applied force of up to 300 nN/μm^2 to transition into successful mono-atomic sheet separation from graphitic material [123]. Further notable limitations are the method's inability for scalability (low throughput) and reproducibility [124].

7.1.6. Chemical and Electrochemical Exfoliation

The exfoliations of the graphite to graphene include reduction of the van de Waals forces (~ 61 meV per C atom) between graphite, thus resulting in gradual interlayer spacing. Briefly, the exfoliation through an ultrasonicated liquid phase and electrochemical set up is based on the large-sized molecule or metallic atom intercalation/insertion within the graphite sheets or via chemical oxidation. The ultrasonication uses waves that have rarefaction and compression cycles. Moreover, the cavitation occurs in the rarefaction phase, whereby negative acoustic pressure is high to disintegrate the liquid forming transient/stable microbubbles. The cavitation also involves the generation and vigorous collapse of the bubble within a short period, with a temperature of up to 5000 K, a heating/cooling rate of up to 10^9 K s^{-1}, and pressure of up to 20 MPa [125]. The process also produces shock waves and hydromechanical forces, which contribute to breaking graphitic bonds. However, the edge defects sourced from cavitation and long sonication period may result in oxygenated graphene edges if sometimes the exfoliation is performed in the air [126].

Due to interlayer spacing and weak van der Waals forces, sonication in different pure solvents and surfactant-assisted solvents have been employed for graphite exfoliation outputting suitable single to few-layer graphene. The yield and quality of the product (lateral size, layer number) depend on sonication time, power, temperature, frequency, and solvent choice [127].

The solvent choice is key to the graphite's liquid phase exfoliation (LPE). It has been documented that solvent mainly affects the graphene colloidal suspension stability and amount. Consequently, the exfoliation depends on the solvent surface tension, and the study showed that 40–50 mJ/m^2 surface tension values tend to output good exfoliation [128]. Secondly, the solvent should overpower the weak forces between graphene sheets, of which these sheets are suspended within the π–π stacking length of 3.35–3.4 Å [120]. Thirdly, to achieve suspension stability, the nanolayer-solvent interactions must balance the interlayer attractive forces [129]. The LPE has been regarded as an efficient graphene synthesis method; interestingly, water can be used in the process. However, surfactant-water-assisted sonication has also been well studied for the betterment of dispersion, exfoliation, layer quality, and yield [130].

The documentation shows a linear proportional growth between the exfoliated graphene layer amount and the applied sonication energy, temperature, power, and frequency [127]. Furthermore, these parameters have shown the potential to produce a few graphene layers [131]. Several studies have been conducted to confirm their effects. However, some studies proved an indirectly proportional relationship between the sonication time and the abovementioned parameters in producing better mono to few-layer graphene.

7.2. Indirect Methods

7.2.1. Epitaxial Growth

Epitaxial graphene growth involves the decomposition of SiC under high temperatures in an ultra-high vacuum. The Si is vaporized, resulting in a carbon-rich surface in graphene layer form on the substrate top surface [122]. Moreover, post the interface layer generation, the Si may be sublimated by the step edges (resulting in horizontal or in-plane diffusion) or through interlayer defects (resulting in vertical diffusion). Four critical steps of epitaxial graphene growth, (a) the interlayer production, (b) graphene sheet growth at step edges, and (c) graphitization (where the step flow front forms toward terraces center, whereas the flakes combine and thus resulting in increased domain sizes), (d) post-formation of the first monolayer graphene then the Si may diffuse via step edges or defects to generate another layer (bilayer) [122]. The epitaxial growth is partitioned into hetero-epitaxial (the film

deposited on the substrate surface is sourced from various materials) and homo-epitaxial growth (the substrate and film are of the same material). This study showed the growth of three few-layered graphenes on single crystalline 6H-SiC, and it was also found that the graphene growth rate on SiC substrate was mainly dependent on a particular SiC crystal face. A further discovery was that graphene growth was slower on the Si-face than on the C-face via thermal decomposition of SiC greater than 1000 °C [132]. Consequently, epitaxial growth on SiC substrate has been regarded as a vital method for the large-scale generation of graphene.

7.2.2. Chemical Vapour Deposition (CVD)

During the CVD, suitable graphene precursors are deposited on the substrate surface via pyrolytic decomposition, thus resulting in deposition sites on the substrate surface and subsequent layer deposition [133]. The method is regarded as an effective procedure for generating better quality graphene with high throughput and the capability to yield large area mono crystal graphene [134]. In this method, the resultant toxic by-products are eliminated from the reaction body via flow gas, enabling proper disposal. Despite the merits of CVD, the limitations are: the employed precursors should be readily volatile for deposition on the substrate surface, expensiveness, and consumption of high substrate amount to achieve large throughput of the graphene sheet [135].

7.2.3. Carbon Nanotube (CNT)

CNTs are cylindrical macromaterial composed of hexagonal lattice carbon atom arrangement forming a tube-like structure [115]. The carbon atom hybridization in the CNT sheet results in two types of CNTs: single-wall carbon nanotubes (SWCNT) and multi-wall carbon nanotubes (MWCNTs). The SWCNT can be seen as a cylindrically rolled single graphene sheet with a diameter of 1 to 3 nm. In contrast, the MWCNTs (1 to 100 nm) are composed of several diametric SWCNTs compressed together, forming multi-layered and rolled graphene sheets [136]. Carbon can create geometrical structuring through its binding strength for the generation of long-chain and branched molecules. CNTs possess good properties like ultra-light mass, thermal stability, surface area, mechanical strength, and thermal stability [137]. Due to the CNTs' exceptional properties, the material has stretched application in supporting agents in hybrid nanocomposite material, biosensors, and fuel cells [138]. The CNTs' porous nature and high specific surface area have made several study explorations on CNTs for remediation of organic, microbes, and inorganic water pollutants. Since its discovery in 1991, the configured CNTs have attracted research studies for Cr, Fe, Cu, Pb, Cd, and Zn removal in simulated and real wastewater by adsorption mechanism [139].

To achieve CNTs' optimum performance, several synthesis methods have been employed. Some are common to the graphene synthesis method previously covered in this review. The methods are electric arc discharge, laser ablation, chemical vapor deposition, vapor phase growth, thermal synthesis, and flame synthesis [140].

Vapour phase growth is a modified and more developed version of the chemical vapor deposition method. The method has a ferrocene catalyst and two furnaces in the reaction chamber with low-temperature values. Additionally, the catalytic particles are generated at furnace one, and their transition to furnace two, the carbon is transported in catalyst via diffusion resulting in CNTs formation [139]. Generally, the CNTs are formed in a reaction chamber with substrate absence and catalytic transitional metal presence. The flame synthesis CNTs method uses the flame as heat energy and nano atom sources. The injection of gaseous catalyst species may functionalize the flame. This method involves heating fuel species in an ambient environment to yield radicals, H_2O vapors, C_2H_2, C_2H_6, H_2, CO, and CO_2 [141]. The CNTs growth is similar to the chemical vapor deposition technique. High-temperature use and high costliness are limitations.

Another method for CNTs synthesis is thermal synthesis. The process involves a steady heat supply which is preferably below 1200 °C. The operation is almost the same

as the chemical vapor deposition but depends on the precursors used in forming CNTs. Transitional metals such as nickel and iron are used as a catalyst in this process [142].

Common synthesis of the CNTs is associated with chemical vapor deposition, laser ablation, and arc discharge [143]. Catalyst precursor and non-catalyzed arc discharge method may be used for CNTs synthesis. Typically, the non-catalyzed synthesis favors MWCNTs, while the catalyst-assisted method suits SWCNTs sourced from metals, graphite, and metal alloys under an inert gas environment [123]. The advantages associated with the methods are better diameter size (<25 nm), larger surface area, and production yield (~99%) with high-purity CNTs. However, the presented disadvantages are high energy consumption, difficult control over the process, tangled CNTs, and low production rate [142].

8. Conclusions

Portable water provision from the heavily polluted industrial wastewater is one of the most critical priorities of the current generation. Applying suitable adsorbents in wastewater treatment has proved very efficient and economical. The current review provided an overview of adsorption processes for contaminant removal. This includes a discussion of the important conventional and non-conventional adsorbents used to remove toxic pollutants from wastewater. The non-conventional adsorbents offer comparative advantages in cost-effectiveness and efficiency.

Likewise, a summary of the development of traditional and nano-advanced adsorbents has been provided in the current review. Various methods have individual significance and drawbacks on material synthesis, affecting the adsorbent performance on metal removal. Thus, moderate adjustments and optimizations are necessary for inexpensive, eco-friendly adsorbent growth. The adsorption process is also affected by material porosity, surface area, affinitive functional group sites, adsorbate-adsorbent interaction, solution pH, ionic strength, adsorbent dosage, and temperature. Furthermore, the adsorption isotherm and kinetic models are vital for the improved adsorption design and monitoring of mono and multilayer adsorption systems. The traditional materials also present a capability for metal uptake in an aqueous environment. The preservation of the small size, surface area, morphology, and magnetic properties of nanomaterials could afford the adsorbent regeneration and reuse. Carbon-based composite material exhibits better adsorption capacities due to their possible functionalization and robustness and offer multiple binding sites for physical or chemical adsorption of the metal species. Likewise, Bio sorbent is an excellent adsorbent with the capability for nonselective toxic metal uptake from the complex matrix. Its cost-effectiveness is a turning point in sorption technology. Besides, it is regeneratable, readily available, and produces near zero quantity of sludge. The application of biosorbents as green technology is therefore essential for the enhancement of the process of wastewater remediation using sorption technology.

Funding: This research was funded by National Research Foundation (NRF), South Africa, grant number: 120375 and Tertiary Education Support Program (TESP), Eskom Holdings SOC Limited Reg No 2002/015527/0.

Data Availability Statement: Not applicable.

Conflicts of Interest: The authors declare no conflict of interest.

References

1. Sharma, M.; Kalita, P.; Senapati, K. Study on Magnetic Materials for Removal of Water Pollutants. In *Emerging Pollutants-Some Strategies for the Quality Preservation of Our Environment*; BoD—Books on Demand: Norderstedt, Germany, 2018; pp. 221–244.
2. Azimi, A.; Azari, A.; Rezakazemi, M.; Ansarpour, M. Removal of Heavy Metals from Industrial Wastewaters: A Review. *ChemBioEng Rev.* **2017**, *4*, 37–59. [CrossRef]
3. Barakat, M.A. New trends in removing heavy metals from industrial wastewater. *Arab. J. Chem.* **2011**, *4*, 361–377. [CrossRef]
4. Fu, F.; Wang, Q. Removal of heavy metal ions from wastewaters: A review. *J. Environ. Manag.* **2011**, *92*, 407–418. [CrossRef] [PubMed]

5. Periyasamy, S.; Kumar, I.A.; Viswanathan, N. Activated Carbon from Different Waste Materials for the Removal of Toxic Metals. *Green Mater. Wastewater Treat.* **2020**, *38*, 47–68. [CrossRef]
6. Alloway, B.J. Sources of Heavy Metals and Metalloids in Soils. In *Heavy Metals in Soils*; Springer: Dordrecht, The Netherlands, 2013; pp. 11–50. [CrossRef]
7. Uddin, M.K. A review on the adsorption of heavy metals by clay minerals, with special focus on the past decade. *Chem. Eng. J.* **2017**, *308*, 438–462. [CrossRef]
8. Sankaran, R.; Show, P.L.; Ooi, C.-W.; Ling, T.C.; Shu-Jen, C.; Chen, S.-Y.; Chang, Y.-K. Feasibility assessment of removal of heavy metals and soluble microbial products from aqueous solutions using eggshell wastes. *Clean Technol. Environ. Policy* **2020**, *22*, 773–786. [CrossRef]
9. Sachan, D.; Ramesh, A.; Das, G. Green synthesis of silica nanoparticles from leaf biomass and its application to remove heavy metals from synthetic wastewater: A comparative analysis. *Environ. Nanotechnol. Monit. Manag.* **2021**, *16*, 100467. [CrossRef]
10. Sharma, R.K.; Solanki, K.; Dixit, R.; Sharma, S.; Dutta, S. Nanoengineered iron oxide-based sorbents for separation of various water pollutants: Current status, opportunities and future outlook. *Environ. Sci. Water Res. Technol.* **2021**, *7*, 818–860. [CrossRef]
11. Abdullah, N.; Yusof, N.; Lau, W.J.; Jaafar, J.; Ismail, A.F. Recent trends of heavy metal removal from water/wastewater by membrane technologies. *J. Ind. Eng. Chem.* **2019**, *76*, 17–38. [CrossRef]
12. Zamora-Ledezma, C.; Negrete-Bolagay, D.; Figueroa, F.; Zamora-Ledezma, E.; Ni, M.; Alexis, F.; Guerrero, V.H. Heavy metal water pollution: A fresh look about hazards, novel and conventional remediation methods. *Environ. Technol. Innov.* **2021**, *22*, 101504. [CrossRef]
13. Chai, W.S.; Cheun, J.Y.; Kumar, P.S.; Mubashir, M.; Majeed, Z.; Banat, F.; Ho, S.H.; Show, P.L. A review on conventional and novel materials towards heavy metal adsorption in wastewater treatment application. *J. Clean. Prod.* **2021**, *296*, 126589. [CrossRef]
14. Qu, J. Research progress of novel adsorption processes in water purification: A review. *J. Environ. Sci.* **2008**, *20*, 1–13. [CrossRef]
15. Jawed, A.; Saxena, V.; Pandey, L.M. Engineered nanomaterials and their surface functionalization for the removal of heavy metals: A review. *J. Water Process. Eng.* **2020**, *33*, 101009. [CrossRef]
16. Fato, F.P.; Li, D.-W.; Zhao, L.-J.; Qiu, K.; Long, Y.-T. Simultaneous Removal of Multiple Heavy Metal Ions from River Water Using Ultrafine Mesoporous Magnetite Nanoparticles. *ACS Omega* **2019**, *4*, 7543–7549. [CrossRef]
17. Tripathi, A.; Rawat Ranjan, M. Heavy Metal Removal from Wastewater Using Low Cost Adsorbents. *J. Bioremediat. Biodegrad.* **2015**, *6*, 315. [CrossRef]
18. Al-Ghouti, M.A.; Da'ana, D.A. Guidelines for the use and interpretation of adsorption isotherm models: A review. *J. Hazard. Mater.* **2020**, *393*, 122383. [CrossRef]
19. Agboola, O.D.; Benson, N.U. Physisorption and Chemisorption Mechanisms Influencing Micro (Nano) Plastics-Organic Chemical Contaminants Interactions: A Review. *Front. Environ. Sci.* **2021**, 167. [CrossRef]
20. Tamiru, M.; Bekele, G. International Journal of Water and Wastewater Treatment Various Absorbents and Parameters Affecting Removal of Water Hardness from Wastewater: Review. *Int. J. Water Wastewater Treat.* **2020**, *6*, 173. [CrossRef]
21. De Freitas, G.R.; da Silva, M.G.C.; Vieira, M.G.A. Biosorption technology for removal of toxic metals: A review of commercial biosorbents and patents. *Environ. Sci. Pollut. Res.* **2019**, *26*, 19097–19118. [CrossRef]
22. Ugwu, E.I.; Tursunov, O.; Kodirov, D.; Shaker, L.M.; Al-Amiery, A.A.; Yangibaeva, I.; Shavkarov, F. Adsorption mechanisms for heavy metal removal using low cost adsorbents: A review. *IOP Conf. Ser. Earth Environ. Sci.* **2020**, *614*, 012166. [CrossRef]
23. Gupta, A.; Sharma, V.; Sharma, K.; Kumar, V.; Choudhary, S.; Mankotia, P.; Kumar, B.; Mishra, H.; Moulick, A.; Ekielski, A.; et al. A Review of Adsorbents for Heavy Metal Decontamination: Growing Approach to Wastewater Treatment. *Materials* **2021**, *14*, 4702. [CrossRef] [PubMed]
24. Vo, T.S.; Hossain, M.M.; Jeong, H.M.; Kim, K. Heavy metal removal applications using adsorptive membranes. *Nano Converg.* **2020**, *7*, 36. [CrossRef] [PubMed]
25. Zand, A.D.; Abyaneh, M.R. Adsorption of Lead, manganese, and copper onto biochar in landfill leachate: Implication of non-linear regression analysis. *Sustain. Environ. Res.* **2020**, *30*, 18. [CrossRef]
26. Burakov, A.E.; Galunin, E.V.; Burakova, I.V.; Kucherova, A.E.; Agarwal, S.; Tkachev, A.G.; Gupta, V.K. Adsorption of heavy metals on conventional and nanostructured materials for wastewater treatment purposes: A review. *Ecotoxicol. Environ. Saf.* **2018**, *148*, 702–712. [CrossRef]
27. Crini, G.; Lichtfouse, E.; Wilson, L.D.; Morin-Crini, N. Conventional and non-conventional adsorbents for wastewater treatment. *Environ. Chem. Lett.* **2019**, *17*, 195–213. [CrossRef]
28. Bushra, R.; Shahadat, M.; Ahmad, A.; Nabi, S.A.; Umar, K.; Oves, M.; Raeissi, A.S.; Muneer, M. Synthesis, characterization, antimicrobial activity and applications of polyanilineTi(IV)arsenophosphate adsorbent for the analysis of organic and inorganic pollutants. *J. Hazard. Mater.* **2014**, *264*, 481–489. [CrossRef]
29. Ayranci, E.; Duman, O. In-Situ UV-Visible Spectroscopic Study on the Adsorption of some Dyes onto Activated Carbon Cloth. *Sep. Sci. Technol.* **2009**, *44*, 3735–3752. [CrossRef]
30. Deliyanni, E.A.; Kyzas, G.Z.; Triantafyllidis, K.S.; Matis, K.A. Activated carbons for the removal of heavy metalions: A systematic review of recent literaturefocused on lead and arsenic ion. *Open Chem.* **2015**, *13*, 699–708.
31. Shehzad, A.; Bashir, M.J.K.; Sethupathi, S.; Lim, J.W. An overview of heavily polluted landfill leachate treatment using food waste as an alternative and renewable source of activated carbon. *Process. Saf. Environ. Prot.* **2015**, *98*, 309–318. [CrossRef]

32. Heidarinejad, Z.; Dehghani, M.H.; Heidari, M.; Javedan, G.; Ali, I.; Sillanpää, M. Methods for preparation and activation of activated carbon: A review. *Environ. Chem. Lett.* **2020**, *18*, 393–415. [CrossRef]
33. Nabais, J.V.; Carrott, P.; Ribeiro Carrott, M.M.L.; Luz, V.; Ortiz, A.L. Influence of preparation conditions in the textural and chemical properties of activated carbons from a novel biomass precursor: The coffee endocarp. *Bioresour. Technol.* **2008**, *99*, 7224–7231. [CrossRef]
34. Deng, H.; Yang, L.; Tao, G.; Dai, J. Preparation and characterization of activated carbon from cotton stalk by microwave assisted chemical activation—Application in methylene blue adsorption from aqueous solution. *J. Hazard. Mater.* **2009**, *166*, 1514–1521. [CrossRef]
35. Tran, H.N.; Chao, H.P.; You, S.J. Activated carbons from golden shower upon different chemical activation methods: Synthesis and characterizations. *Adsorpt. Sci. Technol.* **2017**, *36*, 95–113. [CrossRef]
36. Gao, Y.; Yue, Q.; Gao, B.; Li, A. Insight into activated carbon from different kinds of chemical activating agents: A review. *Sci. Total Environ.* **2020**, *746*, 141094. [CrossRef]
37. Salman, S.; Rasheed, I.; Mohammed, A. IOP Conference Series: Earth and Environmental Science. *IOP Conf. Ser. Earth Environ. Sci.* **2021**, *779*, 012074. [CrossRef]
38. Gebretsadik, H.; Gebrekidan, A.; Demlie, L. Removal of heavy metals from aqueous solutions using Eucalyptus Camaldulensis: An alternate low cost adsorbent. *Cogent Chem.* **2020**, *6*, 1720892. [CrossRef]
39. Rashed, M.; Soltan, M.; Ahmed, M.; Abdou, A. Heavy Metals Removal from Wastewater by Adsorption on Modified Physically Activated Sewage Sludge. *Arch. Org. Inorg. Chem. Sci.* **2018**, *1*, 1–8. [CrossRef]
40. Ibrahim, W.M.; Hassan, A.F.; Azab, Y.A. Biosorption of toxic heavy metals from aqueous solution by Ulva lactuca activated carbon. *Egypt. J. Basic Appl. Sci.* **2019**, *3*, 241–249. [CrossRef]
41. Hernández-Montoya, V.; García-Servin, J.; Bueno-López, J.I. Thermal Treatments and Activation Procedures Used in the Preparation of Activated Carbons. In *Lignocellulosic Precursors Used in the Synthesis of Activated Carbon-Characterization Techniques and Applications in the Wastewater Treatment*; BoD—Books on Demand: Norderstedt, Germany, 2012; pp. 19–36.
42. Tasić, Ž.Z.; Bogdanović, G.D.; Antonijević, M.M. Application of natural zeolite in wastewater treatment: A review. *J. Min. Metall. A Min.* **2019**, *55*, 67–79. [CrossRef]
43. Salih, A.M. *The Purification of Industrial Wastewater to Remove Heavy Metals and Investigation into the Use of Zeolite as a Remediation Tool*; University of Wolverhampton: Wolverhampton, UK, 2017.
44. Turksoy, R.; Terzioglu, G.; Ertugrul Yalcin, I.; Turksoy Terzioglu, O.; Demir, G. Removal of heavy metals from textile industry wastewater. *Front. Life Sci. Relat. Technol.* **2021**, *2*, 44–50. [CrossRef]
45. Taamneh, Y.; Sharadqah, S. The removal of heavy metals from aqueous solution using natural Jordanian zeolite. *Appl. Water Sci.* **2017**, *7*, 2021–2028. [CrossRef]
46. Gülen, J.; Zorbay, F.; Arslan, S. Zeolites and their uses. *Karaelmas J. Sci. Eng.* **2012**, *2*, 63–68.
47. Yuna, Z. Review of the natural, modified, and synthetic zeolites for heavy metals removal from wastewater. *Environ. Eng. Sci.* **2016**, *33*, 443–454. [CrossRef]
48. La Vega, D.P.D.; González, C.; Escalante, C.A.; Gallego, J.; Salamanca, M.; Manrique-Losada, L. Use of faujasite-type zeolite for ion adsorption in municipal wastewater. *Tecnol. Cienc. Agua* **2018**, *9*, 184–208. [CrossRef]
49. Iqra, J.; Faryal, M.; Uzaira, R.; Noshaba, T. Preparation of zeolite from incinerator ash and its application for the remediation of selected inorganic pollutants: A greener approach. *IOP Conf. Ser. Mater. Sci. Eng.* **2014**, *60*, 012060. [CrossRef]
50. Hanane, B.; Seyd Abdelkader, H.; Kromia, M.; Salah, A.M. Removal of Heavy Metals from an Industrial Effluent by Synthesized Zeolite: Case of Bounoura Industrial Zone. *Leban. Sci. J.* **2020**, *21*, 80–94. [CrossRef]
51. Ismail, A.I.M.; El-Shafey, O.I.; Amr, M.H.A.; El-Maghraby, M.S. Pumice Characteristics and Their Utilization on the Synthesis of Mesoporous Minerals and on the Removal of Heavy Metals. *Int. Sch. Res. Not.* **2014**, *2014*, 259379. [CrossRef]
52. Wołowicz, A.; Wawrzkiewicz, M. Screening of Ion Exchange Resins for Hazardous Ni(II) Removal from Aqueous Solutions: Kinetic and Equilibrium Batch Adsorption Method. *Processes* **2021**, *9*, 285. [CrossRef]
53. Gu, S.; Kang, X.; Wang, L.; Lichtfouse, E.; Wang, C. Clay mineral adsorbents for heavy metal removal from wastewater: A review. *Environ. Chem. Lett.* **2018**, *17*, 629–654. [CrossRef]
54. Tripathi, A.K.; Upadhyay, S.; Bhuiyan, M.; Bhattacharya, P.R. A review on prospects of essential oils as biopesticide in insect-pest management. *J. Pharmacogn. Phyther.* **2009**, *1*, 52–63. Available online: http://www.academicjournals.org/jpp (accessed on 10 July 2022).
55. Nakato, T.; Miyamoto, N. Liquid Crystalline Behavior and Related Properties of Colloidal Systems of Inorganic Oxide Nanosheets. *Materials* **2009**, *2*, 1734–1761. [CrossRef]
56. Ayalew, A.A. A critical review on clay-based nanocomposite particles for application of wastewater treatment. *Water Sci. Technol.* **2022**, *85*, 3002–3022. [CrossRef]
57. Bhattacharyya, K.G.; Gupta, S. Sen Adsorption of a few heavy metals on natural and modified kaolinite and montmorillonite: A review. *Adv. Colloid Interface Sci.* **2008**, *140*, 114–131. [CrossRef]
58. Heller-Kallai, L. Thermally Modified Clay Minerals. *Dev. Clay Sci.* **2006**, *1*, 289–308. [CrossRef]
59. Barakan, S.; Aghazadeh, V. The advantages of clay mineral modification methods for enhancing adsorption efficiency in wastewater treatment: A review. *Environ. Sci. Pollut. Res.* **2020**, *28*, 2572–2599. [CrossRef]

60. El Mouzdahir, Y.; Elmchaouri, A.; Mahboub, R.; Gil, A.; Korili, S.A. Equilibrium modeling for the adsorption of methylene blue from aqueous solutions on activated clay minerals. *Desalination* **2010**, *250*, 335–338. [CrossRef]
61. Akar, S.T.; Yetimoglu, Y.; Gedikbey, T. Removal of chromium (VI) ions from aqueous solutions by using Turkish montmorillonite clay: Effect of activation and modification. *Desalination* **2009**, *244*, 97–108. [CrossRef]
62. Shawabkeh, A.; Al-Khashman, O.; Al-Omari, H.; Shawabkeh, A. Cobalt and zinc removal from aqueous solution by chemically treated bentonite. *Environmentalist* **2007**, *27*, 357. [CrossRef]
63. Komadel, P.; Madejová, J. Acid Activation of Clay Minerals. *Dev. Clay Sci.* **2013**, *5*, 385–409. [CrossRef]
64. Borji, H.; Ayoub, G.M.; Bilbeisi, R.; Nassar, N.; Malaeb, L. How Effective Are Nanomaterials for the Removal of Heavy Metals from Water and Wastewater? *Water Air Soil Pollut.* **2020**, *231*, 330. [CrossRef]
65. Sinha Ray, S.; Okamoto, M. Polymer/layered silicate nanocomposites: A review from preparation to processing. *Prog. Polym. Sci.* **2003**, *28*, 1539–1641. [CrossRef]
66. Bhati, M.; Rai, R. Nanotechnology and water purification: Indian know-how and challenges. *Environ. Sci. Pollut. Res.* **2017**, *24*, 23423–23435. [CrossRef]
67. Kolluru, S.S.; Agarwal, S.; Sireesha, S.; Sreedhar, I.; Kale, S.R. Heavy metal removal from wastewater using nanomaterials-process and engineering aspects. *Process. Saf. Environ. Prot.* **2021**, *150*, 323–355. [CrossRef]
68. Liosis, C.; Papadopoulou, A.; Karvelas, E.; Karakasidis, T.E.; Sarris, I.E. Heavy Metal Adsorption Using Magnetic Nanoparticles for Water Purification: A Critical Review. *Materials* **2021**, *14*, 7500. [CrossRef]
69. Saharan, P.; Chaudhary, G.R.; Mehta, S.K.; Umar, A. Removal of water contaminants by iron oxide nanomaterials. *J. Nanosci. Nanotechnol.* **2014**, *14*, 627–643. [CrossRef]
70. Tsedenbal, B.; Lee, J.E.; Huh, S.H.; Koo, B.H.; Lee, C.G. Removal of Heavy Metals from Wastewater using α-Fe2O3 Nanocrystals. *Korean J. Mater. Res.* **2020**, *30*, 447–452. [CrossRef]
71. Jiang, W.; Pelaez, M.; Dionysiou, D.D.; Entezari, M.H.; Tsoutsou, D.; O'Shea, K. Chromium(VI) removal by maghemite nanoparticles. *Chem. Eng. J.* **2013**, *222*, 527–533. [CrossRef]
72. Parvin, F.; Rikta, S.Y.; Tareq, S.M. Application of Nanomaterials for the Removal of Heavy Metal from Wastewater. In *Nanotechnology in Water and Wastewater Treatment: Theory and Applications*; Elsevier: Amsterdam, The Netherlands, 2019; pp. 137–157.
73. Tamjidi, S.; Esmaeili, H.; Moghadas, B.K. Application of magnetic adsorbents for removal of heavy metals from wastewater: A review study. *Mater. Res. Express* **2019**, *6*, 102004. [CrossRef]
74. Vojoudi, H.; Badiei, A.; Bahar, S.; Mohammadi Ziarani, G.; Faridbod, F.; Ganjali, M.R. A new nano-sorbent for fast and efficient removal of heavy metals from aqueous solutions based on modification of magnetic mesoporous silica nanospheres. *J. Magn. Magn. Mater.* **2017**, *441*, 193–203. [CrossRef]
75. Lingamdinne, L.P.; Chang, Y.Y.; Yang, J.K.; Singh, J.; Choi, E.H.; Shiratani, M.; Koduru, J.R.; Attri, P. Biogenic reductive preparation of magnetic inverse spinel iron oxide nanoparticles for the adsorption removal of heavy metals. *Chem. Eng. J.* **2017**, *307*, 74–84. [CrossRef]
76. Mahmoud, M.E.; Abdelwahab, M.S.; Abdou, A.E.H. Enhanced removal of lead and cadmium from water by Fe3O4-cross linked-O-phenylenediamine nano-composite. *Sep. Sci. Technol.* **2015**, *51*, 237–247. [CrossRef]
77. Giraldo, L.; Erto, A.; Moreno-Piraján, J.C. Magnetite nanoparticles for removal of heavy metals from aqueous solutions: Synthesis and characterization. *Adsorption* **2013**, *19*, 465–474. [CrossRef]
78. Shahzad, A.; Miran, W.; Rasool, K.; Nawaz, M.; Jang, J.; Lim, S.-R.; Lee, D.S. Heavy metals removal by EDTA-functionalized chitosan graphene oxide nanocomposites. *RSC Adv.* **2017**, *7*, 9764. [CrossRef]
79. Zawrah, M.F.; El Shereefy, E.S.E.; Khudir, A.Y. Reverse Precipitation Synthesis of ≤10 nm Magnetite Nanoparticles and Their Application for Removal of Heavy Metals from Water. *Silicon* **2018**, *11*, 85–104. [CrossRef]
80. Muhajir, M.; Puspitasari, P.; Razak, J.A. Synthesis and Applications of Hematite α-Fe2O3: A Review. *J. Mech. Eng. Sci. Technol.* **2020**, *3*, 51–58. [CrossRef]
81. Basavegowda, N.; Mishra, K.; Lee, Y.R. Synthesis, characterization, and catalytic applications of hematite (α-Fe2O3) nanoparticles as reusable nanocatalyst. *Adv. Nat. Sci. Nanosci. Nanotechnol.* **2017**, *8*, 025017. [CrossRef]
82. Davarnejad, R.; Nikandam, K. *Zinc Oxide Nanoparticles Preparation for Pd2+ Ions Adsorption from Aqueous Wastewaters: A Green Technique*; Research Square: Durham, NC, USA, 2021. [CrossRef]
83. Yu, G.; Lu, Y.; Guo, J.; Patel, M.; Bafana, A.; Wang, X.; Qiu, B.; Jeffryes, C.; Wei, S.; Guo, Z.; et al. Carbon nanotubes, graphene, and their derivatives for heavy metal removal. *Mater. Sci.* **2017**, *1*, 56–78. [CrossRef]
84. Grover, V.A.; Hu, J.; Engates, K.E.; Shipley, H.J. Adsorption and desorption of bivalent metals to hematite nanoparticles. *Environ. Toxicol. Chem.* **2012**, *31*, 86–92. [CrossRef]
85. Marcus, M.; Karni, M.; Baranes, K.; Levy, I.; Alon, N.; Margel, S.; Shefi, O. Iron oxide nanoparticles for neuronal cell applications: Uptake study and magnetic manipulations. *J. Nanobiotechnol.* **2016**, *14*, 37. [CrossRef]
86. Badmus, K.O.; Irakoze, N.; Adeniyi, O.R.; Petrik, L. Synergistic advance Fenton oxidation and hydrodynamic cavitation treatment of persistent organic dyes in textile wastewater. *J. Environ. Chem. Eng.* **2020**, *8*, 103521. [CrossRef]
87. Blanchart, P. Extraction, Properties and Applications of Titania. In *Industrial Chemistry of Oxides for Emerging Applications*; John Wiley & Sons, Ltd.: Hoboken, NJ, USA, 2018; pp. 255–309.
88. Rodriguez, A.; Segura, X.; Ferrer, A. *Removal of Cadmium(II), Lead(II) and Chromiun(VI) in Water with Nanomaterials*; Universitat Autonoma de Barcelona: Barcelona, Spain, 2015.

89. Wang, X.; Cai, W.; Lin, Y.; Wang, G.; Liang, C. Mass production of micro/nanostructured porous ZnO plates and their strong structurally enhanced and selective adsorption performance for environmental remediation. *J. Mater. Chem.* **2010**, *20*, 8582–8590. [CrossRef]
90. Máynez-Navarro, O.D.; Sánchez-Salas, J.L. Focus on Zinc Oxide as a Photocatalytic Material for Water Treatment. *Int. J. Bioremediat. Biodegrad.* **2017**, *2018*, 106. [CrossRef]
91. Mohammadi, F.M.; Ghasemi, N. Influence of temperature and concentration on biosynthesis and characterization of zinc oxide nanoparticles using cherry extract. *J. Nanostruct. Chem.* **2018**, *8*, 93–102. [CrossRef]
92. Shaba, E.Y.; Jacob, J.O.; Tijani, J.O.; Suleiman, M.A.T. A critical review of synthesis parameters affecting the properties of zinc oxide nanoparticle and its application in wastewater treatment. *Appl. Water Sci.* **2021**, *11*, 48. [CrossRef]
93. Azizi, S.; Shahri, M.M.; Mohamad, R. Green synthesis of zinc oxide nanoparticles for enhanced adsorption of lead Ions from aqueous solutions: Equilibrium, kinetic and thermodynamic studies. *Molecules* **2017**, *22*, 831. [CrossRef] [PubMed]
94. Çavuş, S.; Gürdağ, G. Noncompetitive Removal of Heavy Metal Ions from Aqueous Solutions by Poly[2-(acrylamido)-2-methyl-1-propanesulfonic acid-co-itaconic acid] Hydrogel. *Ind. Eng. Chem. Res.* **2009**, *48*, 2652–2658. [CrossRef]
95. Thines, R.K.; Mubarak, N.M.; Nizamuddin, S.; Sahu, J.N.; Abdullah, E.C.; Ganesan, P. Application potential of carbon nanomaterials in water and wastewater treatment: A review. *J. Taiwan Inst. Chem. Eng.* **2017**, *72*, 116–133. [CrossRef]
96. Yoo, M.J.; Park, H.B. Effect of hydrogen peroxide on properties of graphene oxide in Hummers method. *Carbon N.Y.* **2019**, *141*, 515–522. [CrossRef]
97. Khan, S.; Achazhiyath Edathil, A.; Banat, F. Sustainable synthesis of graphene-based adsorbent using date syrup. *Sci. Rep.* **2019**, *9*, 18106. [CrossRef]
98. Ahmad, S.Z.N.; Wan Salleh, W.N.; Ismail, A.F.; Yusof, N.; Mohd Yusop, M.Z.; Aziz, F. Adsorptive removal of heavy metal ions using graphene-based nanomaterials: Toxicity, roles of functional groups and mechanisms. *Chemosphere* **2020**, *248*, 126008. [CrossRef]
99. Ijaz, I.; Gilani, E.; Nazir, A.; Bukhari, A. Detail review on chemical, physical and green synthesis, classification, characterizations and applications of nanoparticles. *Green Chem. Lett. Rev.* **2020**, *13*, 59–81. [CrossRef]
100. Ali, I.; Peng, C.; Naz, I.; Amjed, M.A. Water Purification Using Magnetic Nanomaterials: An Overview. In *Nanotechnology in the Life Sciences*; Springer: Cham, Switzerland, 2019; pp. 161–179.
101. Arole, V.M.; Munde, S.V. Fabrication of nanomaterials by top-down and bottom-up approaches—An overview. *JAAST Mater. Sci.* **2014**, *1*, 89–93.
102. Yazid, N.A.; Joon, Y.C. Co-precipitation synthesis of magnetic nanoparticles for efficient removal of heavy metal from synthetic wastewater. *AIP Conf. Proc.* **2019**, *2124*, 020019. [CrossRef]
103. Singh, S.; Barick, K.C.; Bahadur, D. Functional Oxide Nanomaterials and Nanocomposites for the Removal of Heavy Metals and Dyes. *Nanomater. Nanotechnol.* **2013**, *3*, 3–20. [CrossRef]
104. Gallo-Cordova, A.; Morales, M.D.P.; Mazarío, E. Effect of the Surface Charge on the Adsorption Capacity of Chromium(VI) of Iron Oxide Magnetic Nanoparticles Prepared by Microwave-Assisted Synthesis. *Water* **2019**, *11*, 2372. [CrossRef]
105. Müller, B.R. Effect of particle size and surface area on the adsorption of albumin-bonded bilirubin on activated carbon. *Carbon* **2010**, *48*, 3607–3615. [CrossRef]
106. De Gisi, S.; Lofrano, G.; Grassi, M.; Notarnicola, M. Characteristics and adsorption capacities of low-cost sorbents for wastewater treatment: A review. *Sustain. Mater. Technol.* **2016**, *9*, 10–40. [CrossRef]
107. Mbayachi, V.B.; Ndayiragije, E.; Sammani, T.; Taj, S.; Mbuta, E.R. Graphene synthesis, characterization and its applications: A review. *Results Chem.* **2021**, *3*, 100163. [CrossRef]
108. Hua, M.; Zhang, S.; Pan, B.; Zhang, W.; Lv, L.; Zhang, Q. Heavy metal removal from water/wastewater by nanosized metal oxides: A review. *J. Hazard. Mater.* **2012**, *211*, 317–331. [CrossRef]
109. Wu, Y.; Wang, S.; Komvopoulos, K. A review of graphene synthesis by indirect and direct deposition methods. *J. Mater. Res.* **2020**, *35*, 76–89. [CrossRef]
110. Lee, X.J.; Hiew, B.Y.Z.; Lai, K.C.; Lee, L.Y.; Gan, S.; Thangalazhy-Gopakumar, S.; Rigby, S. Review on graphene and its derivatives: Synthesis methods and potential industrial implementation. *J. Taiwan Inst. Chem. Eng.* **2019**, *98*, 163–180. [CrossRef]
111. Karim, M.R.; Hayami, S. Chemical, Thermal, and Light-Driven Reduction of Graphene Oxide: Approach to Obtain Graphene and its Functional Hybrids. In *Graphene Materials—Advanced Applications*; IntechOpen: London, UK, 2017; p. 89.
112. Ali, M.; Urgen, M. *Morphology and Structure of Carbon Films Deposited at Varying Chamber Pressure*; COMSATS University: Islamabad, Pakistan, 2018.
113. Ferreira, F.V.; Franceschi, W.; Menezes, B.R.C.; Biagioni, A.F.; Coutinho, A.R.; Cividanes, L.S. Synthesis, characterization, and applications of carbon nanotubes. In *Carbon-Based Nanofillers and Their Rubber Nanocomposites: Carbon Nano-Objects*; Elsevier: Amsterdam, The Netherlands, 2019; pp. 1–45. [CrossRef]
114. Chen, Y.; Zhao, H.; Sheng, L.; Yu, L.; An, K.; Xu, J.; Ando, Y.; Zhao, X. Mass-production of highly-crystalline few-layer graphene sheets by arc discharge in various H2–inert gas mixtures. *Chem. Phys. Lett.* **2012**, *538*, 72–76. [CrossRef]
115. Shoukat, R.; Khan, M.I. Carbon nanotubes: A review on properties, synthesis methods and applications in micro and nanotechnology. *Microsyst. Technol.* **2021**, *27*, 4183–4192. [CrossRef]
116. Qian, M.; Zhou, Y.S.; Gao, Y.; Park, J.B.; Feng, T.; Huang, S.M.; Sun, Z.; Jiang, L.; Lu, Y.F. Formation of graphene sheets through laser exfoliation of highly ordered pyrolytic graphite. *Appl. Phys. Lett.* **2011**, *98*, 173108. [CrossRef]

117. Wang, J.; Fan, L.; Wang, X.; Xiao, T.; Peng, L.; Wang, X.; Yu, J.; Cao, L.; Xiong, Z.; Fu, Y.; et al. Pulsed laser deposition of monolayer and bilayer graphene. *Appl. Surf. Sci.* **2019**, *494*, 651–658. [CrossRef]
118. Jiang, N.; Li, X.; Guo, H.; Li, J.; Shang, K.; Lu, N.; Wu, Y. Plasma-assisted catalysis decomposition of BPA over graphene-CdS nanocomposites in pulsed gas-liquid hybrid discharge: Photocorrosion inhibition and synergistic mechanism analysis. *Chem. Eng. J.* **2021**, *412*, 128627. [CrossRef]
119. Sadeghi, H.; Solati, E.; Dorranian, D. Producing graphene nanosheets by pulsed laser ablation: Effects of liquid environment. *J. Laser Appl.* **2019**, *31*, 042003. [CrossRef]
120. Kumar, R.; Sahoo, S.; Joanni, E.; Singh, R.K.; Tan, W.K.; Kar, K.K.; Matsuda, A. Recent progress in the synthesis of graphene and derived materials for next generation electrodes of high performance lithium ion batteries. *Prog. Energy Combust. Sci.* **2019**, *75*, 100786. [CrossRef]
121. Bhuyan, M.S.A.; Uddin, M.N.; Islam, M.M.; Bipasha, F.A.; Hossain, S.S. Synthesis of graphene. *Int. Nano Lett.* **2016**, *6*, 65–83. [CrossRef]
122. Yan, Y.; Nashath, F.Z.; Chen, S.; Manickam, S.; Lim, S.S.; Zhao, H.; Lester, E.; Wu, T.; Pang, C.H. Synthesis of graphene: Potential carbon precursors and approaches. *Nanotechnol. Rev.* **2020**, *9*, 1284–1314. [CrossRef]
123. Jiao, L.; Zhang, L.; Wang, X.; Diankov, G.; Dai, H. Narrow graphene nanoribbons from carbon nanotubes. *Nature* **2009**, *458*, 877–880. [CrossRef] [PubMed]
124. Bhoria, R.S. Enhancing liquid phase exfoliation of graphene in organic solvents with additives. In *Graphene and Its Derivatives-Synthesis and Applications*; IntechOpen: London, UK, 2019. [CrossRef]
125. Suslick, K.S.; Crum, L.A. *Sonochemistry and Sonoluminescence*; Springer: Berlin, Germany, 2007; pp. 271–281. [CrossRef]
126. Wei, Y.; Sun, Z. Liquid-phase exfoliation of graphite for mass production of pristine few-layer graphene. Curr. Opin. *Colloid Interface Sci.* **2015**, *20*, 311–321. [CrossRef]
127. Tyurnina, A.V.; Tzanakis, I.; Morton, J.; Mi, J.; Porfyrakis, K.; Maciejewska, B.M.; Grobert, N.; Eskin, D.G. Ultrasonic exfoliation of graphene in water: A key parameter study. *Carbon N.Y.* **2020**, *168*, 737–747. [CrossRef]
128. Bleu, Y.; Bourquard, F.; Tite, T.; Loir, A.S.; Maddi, C.; Donnet, C.; Garrelie, F. Review of graphene growth from a solid carbon source by pulsed laser deposition (PLD). *Front. Chem.* **2018**, *6*, 572. [CrossRef]
129. Hernandez, Y.; Nicolosi, V.; Lotya, M.; Blighe, F.M.; Sun, Z.; De, S.; McGovern, I.T.; Holland, B.; Byrne, M.; Gun'Ko, Y.K.; et al. High-yield production of graphene by liquid-phase exfoliation of graphite. *Nat. Nanotechnol.* **2008**, *3*, 563–568. [CrossRef]
130. Narayan, R.; Kim, S.O. Surfactant mediated liquid phase exfoliation of graphene. *Nano Converg.* **2015**, *2*, 20. [CrossRef]
131. Noroozi, M.; Zakaria, A.; Radiman, S.; Wahab, Z.A. Environmental Synthesis of Few Layers Graphene Sheets Using Ultrasonic Exfoliation with Enhanced Electrical and Thermal Properties. *PLoS ONE* **2016**, *11*, e152699. [CrossRef]
132. Shan, X.; Wang, Q.; Bian, X.; Li, W.; Chen, G.; Zhu, H. Graphene layers on Si-face and C-face surfaces and interaction with Si and C atoms in layer controlled graphene growth on SiC substrates. *RSC Adv.* **2015**, *5*, 78625–78633. [CrossRef]
133. Brisebois, P.P.; Siaj, M. Harvesting graphene oxide—Years 1859 to 2019: A review of its structure, synthesis, properties and exfoliation. *J. Mater. Chem. C* **2020**, *8*, 1517–1547. [CrossRef]
134. Wang, C.; Vinodgopal, K.; Dai, G.-P. *Large-Area Synthesis and Growth Mechanism of Graphene by Chemical Vapor Deposition*; IntechOpen: London, UK, 2018.
135. Saeed, M.; Alshammari, Y.; Majeed, S.A.; Al-Nasrallah, E. Chemical Vapour Deposition of Graphene—Synthesis, Characterisation, and Applications: A Review. *Molecules* **2020**, *25*, 3856. [CrossRef]
136. Bhandari, H.; Garg, S.; Gaba, R. Advanced Nanocomposites for Removal of Heavy Metals from Wastewater. *Macromol. Symp.* **2021**, *397*, 2000337. [CrossRef]
137. Anzar, N.; Hasan, R.; Tyagi, M.; Yadav, N.; Narang, J. Carbon nanotube—A review on Synthesis, Properties and plethora of applications in the field of biomedical science. *Sens. Int.* **2020**, *1*, 100003. [CrossRef]
138. Ates, M.; Eker, A.A.; Eker, B. Carbon nanotube-based nanocomposites and their applications. *J. Adhes. Sci. Technol.* **2017**, *31*, 1977–1997. [CrossRef]
139. Rathinavel, S.; Priyadharshini, K.; Panda, D. A review on carbon nanotube: An overview of synthesis, properties, functionalization, characterization, and the application. *Mater. Sci. Eng. B* **2021**, *268*, 115095. [CrossRef]
140. Hamzah, N.; Yasin, M.F.M.; Yusop, M.Z.M.; Saat, A.; Subha, N.A.M. Rapid production of carbon nanotubes: A review on advancement in growth control and morphology manipulations of flame synthesis. *J. Mater. Chem. A* **2017**, *5*, 25144–25170. [CrossRef]
141. Arora, B.; Attri, P. Carbon Nanotubes (CNTs): A Potential Nanomaterial for Water Purification. *J. Compos. Sci.* **2020**, *4*, 135. [CrossRef]
142. Li, D.; Tong, L. Direct Growth of Carbon Nanotubes on Aluminum Foil by Atmospheric Pressure Microwave Plasma Chemical Vapor Deposition. *Processes* **2020**, *9*, 36. [CrossRef]
143. Szymanski, L.; Kolacinski, Z.; Wiak, S.; Raniszewski, G.; Pietrzak, L. Synthesis of Carbon Nanotubes in Thermal Plasma Reactor at Atmospheric Pressure. *Nanomaterials* **2017**, *7*, 45. [CrossRef]